Pergamon

PII: S0038-1101(96)00083-4

Solid-State Electronics Vol. 39, No. 11, pp. 1629–1636, 1996

0038-1101/96 $15.00 + 0.00

NUMERICAL AND EXPERIMENTAL ANALYSIS OF THE STATIC CHARACTERISTICS AND NOISE IN UNGATED RECESSED MESFET STRUCTURES

J. MATEOS[1], T. GONZÁLEZ[1], D. PARDO[1], P. TADYSZAK[2], F. DANNEVILLE[2] and A. CAPPY[2]

[1]Departamento de Física Aplicada, Universidad de Salamanca, Plaza de la Merced s/n, 37008 Salamanca, Spain

[2]Institut d'Electronique et Microélectronique du Nord, U.M.R. C.N.R.S. no. 9929, Département Hyperfréquences et Semiconducteurs, BP 69, 59652 Villeneuve D'Ascq Cédex, France

(Received 16 January 1996; in revised form 8 March 1996)

Abstract—We present an analysis of the static characteristics and noise in GaAs ungated recessed MESFET structures with different values of recess length according to Monte Carlo simulation and experimental measurements. In order to fit results obtained from Monte Carlo simulation with those of measurements of the static I–V characteristic and high frequency noise in real devices, several real effects have been introduced in the simulated structures. A good agreement has been found. Two interesting effects have been studied: first, the surface potential, which controls current flow through the channel, and second, the presence of high fields under the recess, causing the appearance of hot electrons. We analyze these effects on the I–V curves and the noise of the devices, trying to detect the influence of ballistic transport when decreasing the recess length. Copyright © 1996 Elsevier Science Ltd

1. INTRODUCTION

Computer simulation has played an important role in the development of microelectronics[1,2]. When trying to optimize the performance of a given device there are a lot of parameters which can be modified. The industry is not able to fabricate all possible different devices because of material and time constraints. However, simulations are quite appropriate to this aim. With very low cost and not too much time, it is possible to determine the influence of modifications in a given device. An important problem to be faced is the reliability of these simulations. The Monte Carlo particle technique includes a realistic microscopic description of the carrier transport[3] and therefore it has become a very powerful tool for the simulation of electronic devices. Great efforts have been made to reproduce the experimental results with this technique, but a good agreement has rarely been found. The static characteristics are easier to reproduce, but large difficulties are found when dealing with second-order quantities, as is the case for noise in the devices. Though the phenomenological behavior of the noise has been correctly described[4–7], very few attempts to fit noise measurements have been carried out[8,9]. A lot of real effects not considered in the theory can lead to important discrepancies in the results.

The aim of this paper is to model these real effects by comparing the results obtained from Monte Carlo simulation with experimental measurements and to reproduce the I–V characteristics and noise temperature in real devices. The Monte Carlo method[10] is well suited for this purpose since it does not make any assumption about the behavior of the electrons and noise sources inside the device. A critical requirement for the success of this work is the exact knowledge of the geometry and doping of the real devices. However, to avoid the need of prohibitively large computer resources, some simplifications in the simulated structures have to be made.

In order to overcome the complications involved in the measurements of the usual two-port devices, we will study a simple one-port device: a MESFET without gate. To characterize such a device, only the current and a single noise parameter (the noise temperature) at each biasing point are necessary. Even if we have no gate we maintain the usual recessed geometry[11], which increases the importance on the device behavior of the effects owing to the surface states of the semiconductor at the recess[12]. We have modeled these effects by placing a static surface charge at the recess (and not by a constant potential). In addition high electric fields arise in the channel and as a consequence hot electrons appear. These two interesting effects will affect both the current and the noise of our structures. We have compared three structures with different recess lengths, trying to observe effects due to ballistic electron transport in the channel.

Another difficulty for the device modeling is the uncertainty in the damage produced by the plasma etching process used to make the recess. The transport properties of the GaAs in the channel can

be modified by the introduction of impurities coming from the plasma used to etch the semiconductor and also by enhanced surface effects. Due to this uncertainty we have adjusted the I–V curve to the experimental results by changing the depth of the recess in the simulated structures. Furthermore, we have modeled the resistance of the contacts in the simulation to get closer to the real device. By including all the above real phenomena we have obtained a good agreement between the experimental and simulation results, even for the noise behavior of the devices.

In Section 2 we present the MESFET structures and the measurement technique. The details of the Monte Carlo simulation are discussed in Section 3. The comparison between experimental and Monte Carlo results is presented in Section 4. Finally in Section 5 the main conclusions of our work are drawn.

2. TECHNOLOGY AND MEASUREMENTS

A schematic drawing of the real devices to be analyzed is shown in Fig. 1(a). We will focus on the technological problems involved in the recess fabrication. We have three structures with different values of recess length $L = 0.2$, 0.1 and 0.075 μm. The etching technique used in all of them is plasma etching with $CH_4/H_2/Ar$. The etch rate is about 50 Å min^{-1}. This kind of etching can be considered mainly mechanical, since the plasma is used to give energy to the atoms of GaAs for escaping from the attractive forces of the semiconductor. This process

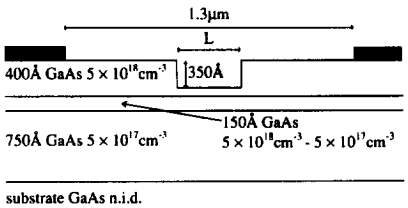

a)

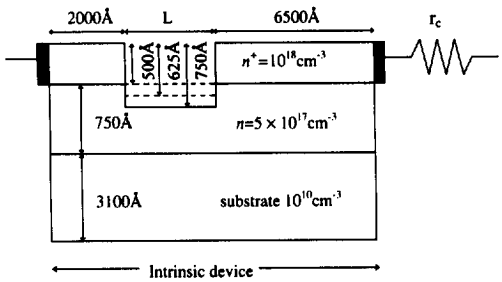

b)

Fig. 1. Scheme of: (a) fabricated; and (b) simulated structures (with three different values of recess depth). The recess length L is variable.

can modify the characteristics of the device in two ways:

(1) The surface of the material will accumulate quite a lot of defects produced by this disordering process. As a result, the amount of surface states can increase and so does the number of charges trapped in these defects and the value of the associated surface potential. Therefore the depletion region under the etched zone may be enlarged, leading to a channel width reduction.

(2) When the semiconductor is exposed to the beam of plasma, some of the molecules of CH_4 arriving to the surface of the material can be implanted in it. These new impurities will change the transport properties of the region where they are present.

The current flowing through the channel is very sensitive to these two effects. We will discuss the way of modeling them in the next section where the details of the Monte Carlo simulation are explained.

The measurement technique used here has been described before[13], but in our case is quite simplified because of the use of one-port devices. Also in Ref. [13] is shown the synopsis of the system used to make the noise measurements. They will be performed in the 2–4 GHz frequency band. This bench contains an automatic network analyzer, a noise receiver and an on-wafer microwave measurement station.

The network analyzer is used to measure the S parameters of:

- the device under test (DUT) S_{DUT};
- the output two-ports S_{OUT} (which represents the probe, the bias tee and the switch);
- the isolator S_{ISO}.

The first step in the process is the calibration of every part of the system. The S_{OUT}, S_{ISO} and Γ_T (reflection coefficient at the noise receiver calibration plane) are measured for every point of frequency. This measurement is made only once since these parameters are constant with the biasing of the DUT. The noise receiver is calibrated with the help of a noise source.

Now we can determine the available noise power of our device (P_{AD}) through the following formula:

$$P_{AD}G_{OUT}G_{ISO} + K_BT(1 - G_{OUT}G_{ISO}) = \frac{P_{AM}|1 - \Gamma_T\Gamma_3|^2}{(1 - |\Gamma_T|^2)(1 - |\Gamma_3|^2)}. \quad (1)$$

P_{AM} is the noise power available at the output. K_B is the Boltzmann constant and T is the room temperature. $K_BT(1 - G_{OUT}G_{ISO})$ is the noise power introduced by the output two-ports and the isolator, whose available gains are G_{OUT} and G_{ISO}, respectively. Γ_T and Γ_3 are the reflection coefficients in both directions at the calibration plane of the noise

receiver (placed just at its input). These four parameters (G_{OUT}, G_{ISO}, Γ_T and Γ_3) can be expressed as a function of S_{DUT}, S_{OUT} and S_{ISO}.

In this way we can extract P_{AD} and the noise temperature of the device T_N ($P_{AD} = K_B T_N$) from the measurement at each frequency (at each biasing) of these two magnitudes: P_{AM} and S_{DUT}. The measured values are constant with frequency (white noise) in the band we have studied, which is between 2 and 4 GHz. All the measurements are performed at room temperature.

3. MONTE CARLO SIMULATION

We have performed the calculations at 300 K using an ensemble Monte Carlo simulation self-consistently coupled with a two-dimensional Poisson solver, and including the effects of a series resistance. The Pauli exclusion principle is considered using the rejection technique described in Ref. [14]. The devices are divided into square cells of 50 × 50 Å (there are two rows of 75 × 50 Å to adjust the depth of the recess). Poisson's equation is solved by using a direct matrix method (LU decomposition), suitable to analyze complicated (recessed) geometries. The number of simulated particles range from 14,300 to 15,000 depending on the structure and the bias point. Ohmic boundary conditions are considered at the contacts, so the number of carriers inside the device is adjusted automatically[15]. The total simulation time is 0.1 ns, divided into time steps of 1 fs each, short enough to get a correct solution of the electric field. The material parameters and the scattering mechanisms of the three valley model (Γ, L and X) used for GaAs have been detailed in previous papers[16, 17].

The scheme of the simulated structures is shown in Fig. 1(b). We have simulated five different structures, three with recess length of $L = 0.2$ μm and depths of 500, 625 and 750 Å (we will call them 1a, 1b and 1c), one with $L = 0.1$ μm and depth of 625 Å (called 2), and finally one with $L = 0.075$ μm and depth of 625 Å (called 3).

The geometry of these structures is a little different to the real one, because of the restrictions of the simulation. Firstly, the contacts are not placed in the surface, but at the sides of the structures, with the aim of reducing the uncertainty in the calculation of the current due to the time discretization of the equations[7]. The regions placed under the contacts in the real devices are ohmic, and in the simulation can be included in the series resistance r_c (together with the contact resistance) with no influence in the results, but leading to an important reduction of the number of simulated particles. This is also the cause of the shortening of the source region, which is an ohmic zone working like a series resistance, and is simulated inside r_c. The drain region cannot be shortened because it is populated by hot carriers which must cover some distance before thermalizing. Another modification in the simulated device is the doping of the n^+-region, which is only 10^{18} cm^{-3} instead of 5×10^{18} cm^{-3}. This lower doping involves no significant change in the results, since the behavior of the device is controlled by the n-region under the channel.

One important feature of our Monte Carlo technique is the incorporation of the series resistance[18], representing the contacts resistance and the nonsimulated ohmic parts of the devices. The value we have taken for r_c is 5×10^{-4} Ω m (where 4×10^{-4} Ω m comes from the contact resistance measured experimentally). In this way the device becomes divided into what we will call intrinsic device, which is simulated through the Monte Carlo technique, and the series resistance.

The way of including the series resistance in the simulation is by changing every time step the voltage applied to the intrinsic device (U_d) depending on the total current flowing through r_c. The differential equation to be solved to calculate U_d is the following[18]:

$$U_d = U_a - r_C I_T = U_a - r_C(I_{cond} + I_{disp}) = U_a - r_C\left(I_{cond} + \frac{\epsilon h}{l}\frac{dU_d}{dt}\right), \quad (2)$$

where U_a is the total biasing, I_T the total current (per unit length in the nonsimulated direction), I_{cond} the conduction current, I_{disp} the displacement current, ϵ the dielectric constant of the material, h the vertical length of the contacts and l the horizontal dimension of the device. The calculation of I_T is performed following Ref. [19]. I_{cond} is given by:

$$I_{cond} = -\frac{q}{lZ}\sum_{i=1}^{N_T} v_i, \quad (3)$$

where q is the absolute value of the electron charge, Z the nonsimulated dimension of the device and v_i the velocity in the x-direction of the electron i. The summation extends to all the carriers inside the device (N_T) at the time considered.

By taking finite differences in eqn (2), the value of U_d at a time t is obtained as:

$$U_d(t) = \frac{U_a - r_C I_{cond} + \frac{r_C \epsilon h}{l\Delta t} U_d(t - \Delta t)}{1 + \frac{r_C \epsilon h}{l\Delta t}}. \quad (4)$$

This calculation assumes a noiseless series resistance. r_C does not add any fluctuation to the total current. It is used only to update the voltage between the electrodes. The noise equivalent circuit of the simulated device (including r_C as noiseless) is shown in Fig. 2(a). S_d and S_S represent the spectral densities of the current density fluctuations in the intrinsic device and in the total circuit, respectively, and r_d the differential resistance of the intrinsic device.

From the total current density fluctuations calculated from the simulation, we extract S_S (as the

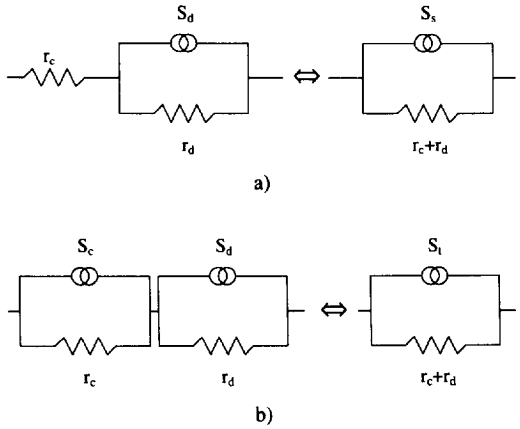

Fig. 2. Noise equivalent circuits: (a) Monte Carlo simulation; (b) Monte Carlo simulation including the noise in the series resistance.

Fourier transform of the autocorrelation function of the fluctuations), and so the noise temperature of the device, T_d, can be easily obtained:

$$S_S = \frac{S_d r_d^2}{(r_c + r_d)^2} = \frac{4K_B T_d r_d}{(r_c + r_d)^2}. \tag{5}$$

However, if we want to compare the results of the simulation with the experimental measurements we must include the effect of the noise generated in the series resistance. We model it as thermal noise at the lattice temperature (T_c) and assume it to be uncorrelated with the noise sources of the intrinsic device. This last assumption may not be completely true, but the influence in the final result is not expected to be significant since r_c is related to ohmic regions far from the active part of the device. The equivalent circuit of the simulation including the noise in the series resistance is presented in Fig. 2(b), where S_c is the spectral density of the noise added by r_c and S_t the total spectral density, whose relation with S_d is:

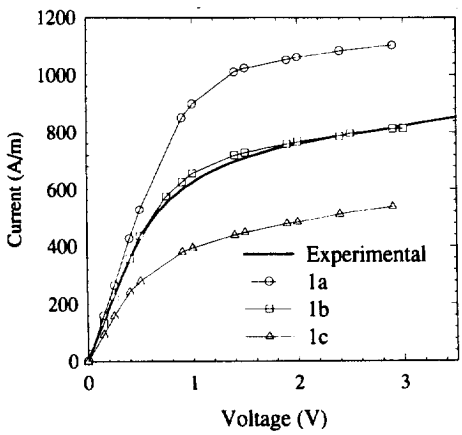

Fig. 3. *I–V* characteristics of the real device with a recess length of 0.2 μm (thick line), compared with simulated results in structures with the same recess length but different depth: 1a, 500 Å (circles); 1b, 625 Å (squares); and 1c, 750 Å (triangles).

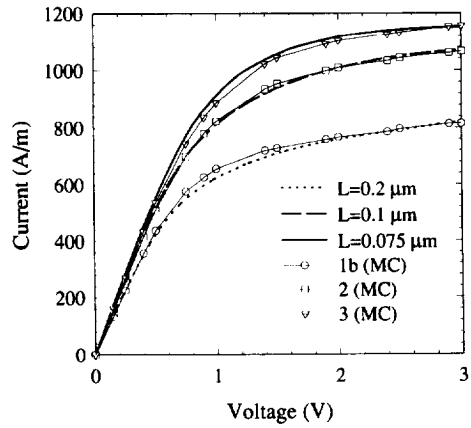

Fig. 4. *I–V* characteristics of the real and simulated structures. The thick lines correspond to the experimental current densities in the devices with a recess length equal to 0.2 μm (dotted), 0.1 μm (dashed) and 0.075 μm (solid), and the symbols to the Monte Carlo simulation in structures with the same recess length: 1b (circles); 2 (squares); and 3 (triangles).

$$S_t = \frac{S_c r_c^2}{(r_c + r_d)^2} + \frac{S_d r_d^2}{(r_c + r_d)^2}$$

$$= \frac{4K_B T_c r_c}{(r_c + r_d)^2} + 4\frac{K_B T_d r_d}{(r_c + r_d)^2}. \tag{6}$$

Knowing the noise temperature of the device, calculated from eqn (5), and the noise temperature of the contacts ($T_c = 300$ K), we can calculate from eqn (6) the noise temperature T_t of the whole device:

$$T_t = \frac{T_c r_c + T_d r_d}{r_c + r_d}, \tag{7}$$

which is the parameter to be compared with the experimental measurement.

The noise temperature is a good magnitude to compare experimental and simulated noise results, because it does not depend on the depth of the device (thus independent of the number of simulated particles). In the case of the spectral density and the correlation function, both change with the nonsimulated dimension of the device. Concerning the dependence of the noise results on the spatial discretization, it has been checked that they are not significantly modified if the size of the meshes is reduced.

Another delicate point in the Monte Carlo simulation is the modeling of the effects related to the surface states at the recess. The perturbation in the periodicity of the lattice potential at the surface introduces energy states lying in the forbidden band. This phenomenon is usually characterized by a surface potential, whose value V_S can be estimated to be -0.5 V in GaAs[20], which produces a depletion of electrons in the zone near the surface. The effects of the surface states are specially critical in the recess surface, since the current flowing through the device is controlled by the width of the channel in this region, which in turn is affected by the surface

potential. Moreover, the plasma etching used to make the recess can accentuate all these phenomena. If we want to simulate structures as similar as possible to the real ones we must include this effect; in any other case the current obtained would be unacceptably high. The way of modeling the surface potential is to place a static surface charge σ at the recess, representing the charge trapped in the surface states, whose value is[21]:

$$\sigma = \sqrt{2qN_D V_s \epsilon}, \tag{8}$$

where q is the absolute value of the electron charge and N_D the impurity density. This model is consistent with the current calculation performed following Ref. [19] since, if the displacement vector outside the device is neglected as compared with its value inside, the surface charge fixes the internal electric field normal to the surface.

The effect of the surface states is considered only in the three walls of the recess since this is the region which controls the current in the device. The inclusion of the surface effects in the rest of the free surface will only lead to an increase of computer time with no significant influence on the results (moreover the surface effects have been reduced in this region because of the passivation process).

In order to include in the Monte Carlo simulation the damage produced by the plasma etching on the region under the recess, we have adjusted the I–V curves of the simulated devices by increasing the depth of the recess (by the same value for the three structures), which represents a similar effect to that produced by this attack. This effect could also be modeled by increasing the amount of surface charge at the recess. However, this would lead to a larger depletion region not only in the direction of the plasma attack (with the same effect of a deeper recess), but also in the direction parallel to the surface (which would appear as a longer recess). This is not justifiable because of the high directivity of the plasma etching, which does not affect intensely the lateral walls of the recess. A more plausible possibility would be the increase of the surface charge only at the bottom of the recess, but this treatment of the channel degradation will not be considered.

4. RESULTS

In Fig. 3 we present the I–V characteristics of the real device with recess length of 0.2 μm compared with the results of the simulation in the structures 1a, 1b and 1c (recess length 0.2 μm and depths of 500, 625 and 700 Å, respectively). The structure 1a has the geometry closest to the real device, but as can be

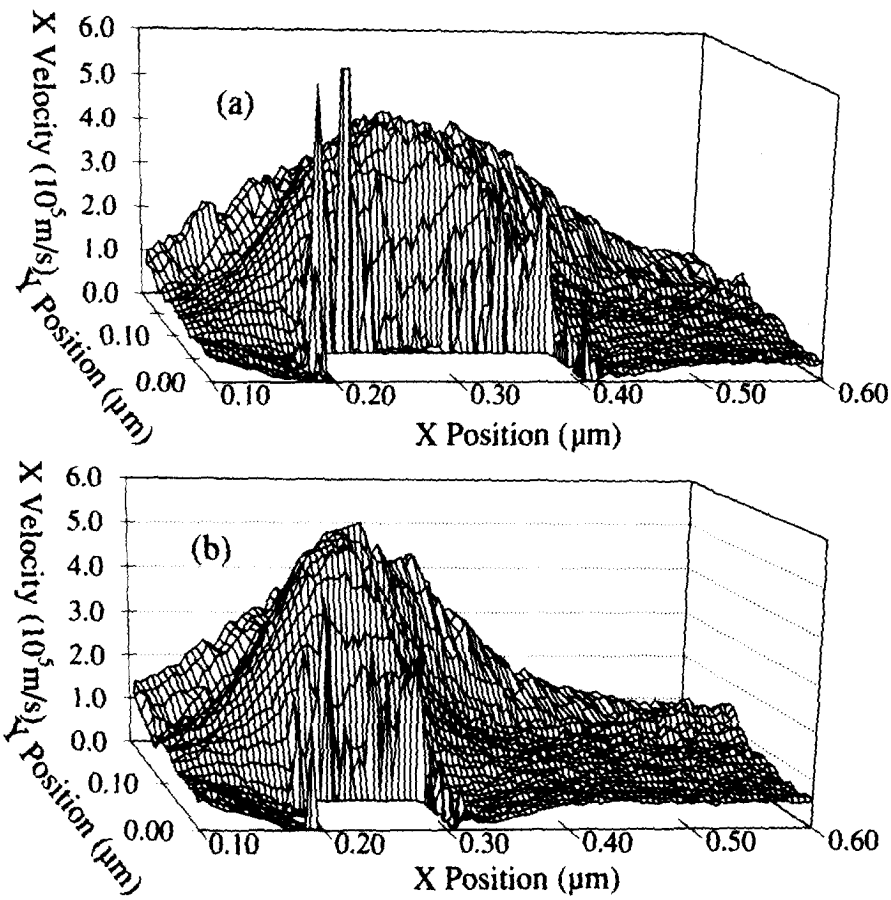

Fig. 5. Average velocity of the electrons inside the structures: (a) 1b and (b) 2. The total biasing is 2.0 V.

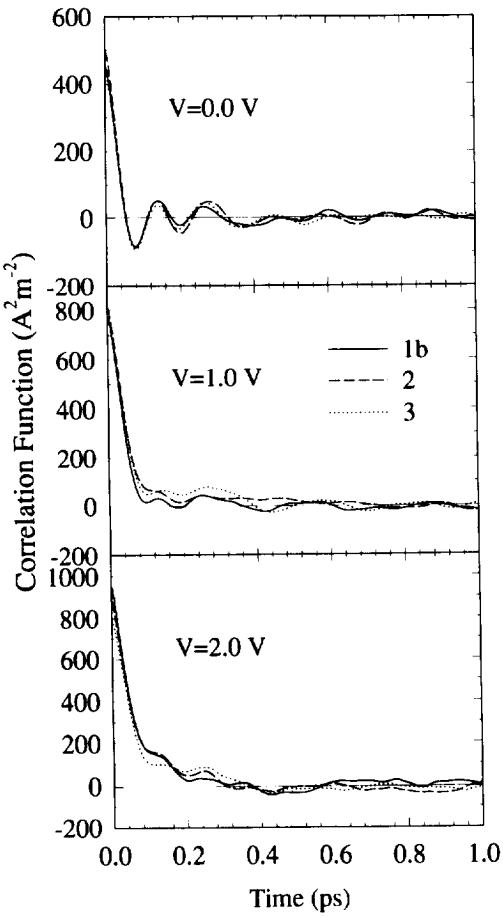

Fig. 6. Autocorrelation function of the total current density fluctuations for the simulated structures 1b (solid), 2 (dashed) and 3 (dotted) for three different bias values: 0 V, 1 V and 2 V.

observed the current obtained is too high. To fit the *I–V* curve we have used the recess depth as an adjustable parameter to take into account the fact that the plasma etching can modify the conducting properties of the region near the recess, as was explained in Section 2. We have obtained a very good agreement in the current with the structure 1b, where the value of the recess depth is 625 Å, higher than in the real structure. This result confirms our assumption. The current of the structure, 1c is too low; however, we will study its noise behavior to see the influence of the recess depth on the noise temperature.

Figure 4 shows the current measured in the three real devices compared with the simulated results in the structures 1b, 2 and 3 (recess length 0.2, 0.1 and 0.075 μm respectively, and all with recess depth equal to 625 Å). We must stress that the same value of the recess depth used to adjust the current in the first device provides also a good agreement in the other cases. This means that the transport is accurately described by the simulation model, and the reason of the disagreement when simulating the real geometry comes from the violent action of the plasma etching. The good agreement obtained for the current in the three structures could not be found by increasing the surface charge as suggested at the end of the last section.

It can be observed that there is an important increase of the current when the recess length is reduced. We can explain this fact from the results of Figs 5(a) and (b), which show the average velocity of electrons inside the structures 1b and 2, under a biasing of 2 V. The increase in the current comes from the higher velocities of the carriers under the recess due to its shorter length (since the width of the channel remains constant). When the recess length is 0.2 μm the maximum velocity in the channel is around 4.5×10^5 m s^{-1}, while reducing the length to 0.1 μm the peak velocity shifts around 5.5×10^5 m s^{-1}. These values remain constant when increasing the applied voltage in the saturation region of the *I–V* curve, which shows that the higher overshoot is not the result of applying the same potential drop over a smaller device, but of the increasing ballistic character of the transport in this region as the recess is shortened. We will try to analyze in the following the effect of this kind of behavior in the noise of the devices.

The simulated autocorrelation functions of the total current density fluctuations for the structures 1b, 2 and 3 under three different biasings are presented in Fig. 6. At equilibrium an oscillatory behavior is observed, with two main frequencies resulting from the coupling of the plasma oscillations caused by the two homojunctions present in the devices [$n^+ - n$ and n-substrate, Fig. 1(b)][4,5]. When the structures are biased, the values of the autocorrelation functions for the shortest times increase and the oscillations vanish. Both effects are attributed to the presence of hot carriers inside the devices. There is no important difference between the

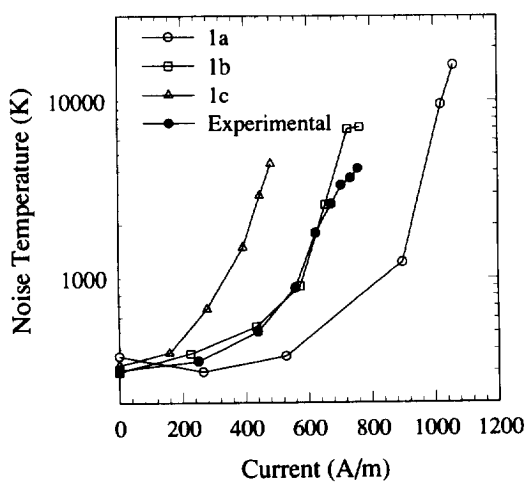

Fig. 7. Experimental noise temperature in the device with a recess length of 0.2 μm (full circles) together with the simulated noise temperature T_i in the structures 1a (open circles), 1b (open squares) and 1c (open triangles).

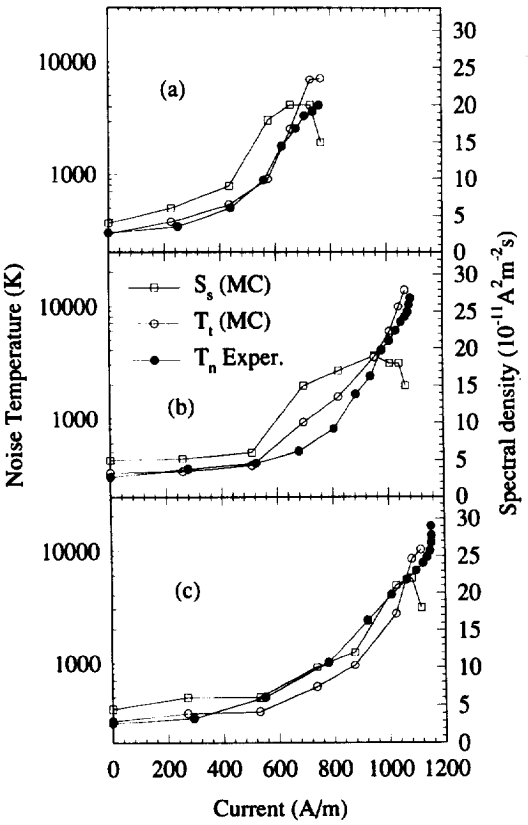

Fig. 8. Value of the spectral density of the current density fluctuations S_S at 2–4 GHz obtained from simulation (open squares, corresponding to the axis on the right), and comparison of the noise temperature obtained from it, T_t (open circles) with the experimental value, T_n (full circles, both corresponding to the axis on the left) in structures with the same recess length: (a) 0.2 μm; (b) 0.1 μm; and (c) 0.075 μm. All simulated structures correspond to a recess depth of 625 Å.

three structures, which means that the associated spectral densities are similar.

To see how the depth of the recess influences the noise temperature we represent in Fig. 7 the values obtained for T_t from the simulation in the structures 1a, 1b and 1c, together with the experimental results in the real device with recess length of 0.2 μm. The values of the noise temperature are highly sensitive to the change of the recess depth, but once the I–V characteristic is fitted (structure 1b) we obtain quite satisfactory results for the noise behavior of the device.

The most valuable results of our study are shown in Fig. 8. They are the simulated low-frequency value of the spectral density of the current density fluctuations S_S and the noise temperature obtained from it T_t, compared with the experimental measurements of the noise temperature T_n in the three real structures, plotted vs the current density. The value of S_S increases with the appearance of the saturation in the current of the device, and then decreases for very high current. In the three structures the shape is similar, with the only difference that the saturation starts at a different current. The error in this result is about 15% due to the long time tail of the autocorrelation functions[5,16]. The accuracy is lower in the values of the noise temperature because of the uncertainty in the calculation of the differential resistance of the device, obtained from the slope of the I–V characteristic. The uncertainty in the experimental results is also of about 15%. Taking this fact into account we can consider that the agreement simulation-measurements is quite good and that we have been able to reproduce the noise behavior of the devices. For the lowest currents, close to equilibrium conditions, the noise temperature takes the expected value of about 300 K. Since the value of the spectral density does not change a lot with the current, the noise behavior of this kind of device is mainly controlled by their resistance, thus making the noise temperature increase when they saturate. Therefore we can extract a qualitative idea of the noise behavior in these structures just from the knowledge of their I–V curves.

Even if we examine carefully these results we cannot find any effect which could be associated to the ballistic transport of electrons under the recess. The behavior of the noise temperature does not change when reducing the recess length within the range analyzed. The noise temperature at equilibrium is that predicted by the Nyquist theorem, and we detect no reduction that could be expected from the ballistic transport[22,23]. This can be attributed to two possible reasons. The length of the recess may be still too long. In addition, it seems that even if the region under the recess is controlling the current, the noise generated in other parts of the device masks the effects of the motion of the electrons in the channel.

5. CONCLUSIONS

We have presented an experimental and theoretical (Monte Carlo simulation) analysis of the static characteristic and high-frequency noise in ungated recessed MESFETs with different geometries. Trying to investigate the effect of ballistic electron transport in the channel the recess length has been reduced down to 0.075 μm. We have made experimental measurements of their I–V characteristic and noise temperature, and next we have tried to reproduce those results using the Monte Carlo method. In order to model several effects which change the ideal behavior of the devices we have modified the standard Monte Carlo technique. We have performed the simulations including a series resistance and surface effects in the recess region.

First we have performed the modeling of the surface effects by means of a static surface charge. Due to the uncertainty in the damage produced by

plasma etching in the conducting channel, the depth of the recess has been used as an adjustable parameter to fit the I–V curves of the real devices. Once this parameter is fixed (to a value higher than the real one), the agreement is very good for all different values of recess length. This means that the transport is accurately described by the model used for GaAs, and one reason of disagreement when simulating the real geometry comes from the violent action of the plasma etching, which degrades the quality of the GaAs under the recess.

Once the I–V curve has been fitted, the noise results are very well reproduced through the Monte Carlo simulation. The noise temperature increases significantly when the current saturates. The latter is associated to the increase of the differential resistance. We have not found any evidence in the noise behavior which could be interpreted as a consequence of ballistic electron transport. Its presence, if it exists in the range of recess lengths analyzed here, is masked by the noise generated in other regions of the devices.

The main achievement of our investigation is that we have been able to reproduce the static and noise experimental results using Monte Carlo simulation, properly modified to include some real effects. This agreement validates our method and motivates us to analyze more complicated and interesting devices. It is also clear from the results that although the Monte Carlo method is able to reproduce very well the qualitative behavior of the devices, in order to reproduce the experimental measurements, mainly of second order quantities, it is necessary to have an exact knowledge of their geometry and the real effects taking place inside.

Acknowledgements—This work has been partially supported by the EC program ELEN through the contract number ERBCHRXCT 920047, and the project TIC95-0652 from the Comisión Interministerial de Ciencia y Tecnología (CICYT).

REFERENCES

1. S. Selberherr, *Analysis and Simulation of Semiconductor Devices*. Springer, Vienna (1984).
2. C. M. Snowden, *Introduction to Semiconductor Device Modeling*. World Scientific, Singapore (1986).
3. C. Jacoboni and P. Lugli, *The Monte Carlo Method for Semiconductor Device Simulation*. Springer, Vienna (1989).
4. L. Varani, L. Reggiani, T. Kuhn, T. González and D. Pardo, *IEEE Trans. Electron. Devices* **4,** 1916 (1994).
5. T. González, D. Pardo, L. Varani and L. Reggiani, *Appl. Phys. Lett.* **63,** 3040 (1993).
6. C. Moglestue, *IEEE Trans. Electron. Devices* **32,** 2092 (1985).
7. T. González, D. Pardo, L. Varani and L. Reggiani, *IEEE Trans. Electron. Devices* **42,** 1991 (1995).
8. J. G. Adams and T. W. Tang, *IEEE Electron Devices Lett.* **13,** 378 (1992).
9. J. G. Adams, T. W. Tang and L. E. Kay, *IEEE Trans. Electron. Devices* **41,** 575 (1994).
10. C. Jacoboni and L. Reggiani, *Rev. Mod. Phys.* **55,** 645 (1983).
11. M. Shur, *GaAs Devices and Circuits*, p. 407. Plenum, New York (1987).
12. P. Kireev, *La Physique des Semiconducteurs*. MIR, Moscow (1975).
13. G. Dambrine, H. Happy, F. Danneville and A. Cappy, *IEEE Trans. Microw. Theory Technol.* **41,** 375 (1993).
14. M. V. Fischetti and S. E. Laux, *Phys. Rev. B* **38,** 9721 (1988).
15. T. González and D. Pardo, *Solid-St. Electron.* **39,** 555 (1996).
16. J. Mateos, T. González and D. Pardo, *J. Appl. Phys.* **77,** 1564 (1995).
17. T. González, J. E. Velázquez, P. M. Gutierrez and D. Pardo, *Semicond. Sci. Technol.* **6,** 862 (1991).
18. V. Mitin, V. Gruzinskis, E. Starikov and P. Shiktorov, *J. Appl. Phys.* **75,** 935 (1994).
19. V. Gruzinskis, S. Kersulis and A. Reklaitis, *Semicond. Sci. Technol.* **6,** 602 (1991).
20. S. G. Pavison and J. D. Devine, *Solid-St. Phys.* **25,** 137 (1970).
21. C. Moglestue, *Monte Carlo Simulation of Semiconductor Devices*, p. 185. Chapman and Hall, London (1993).
22. C. J. Stanton and J. W. Wilkins, *Physica B* **134,** 255 (1985).
23. T. Kuhn, L. Reggiani and L. Varani, *Superlattices Microstruct.* **11,** 205 (1992).